Control of septum thickness by a large protein ring

Michaela Wenzel[1,§,*], Ilkay N. Celik Gulsoy[1*], Yongqiang Gao[1¤], Joost Willemse[2], Mariska G. M. van Rosmalen[3], Gijs J. L. Wuite[3], Wouter H. Roos[4], Leendert W. Hamoen[1#]

[1]Bacterial Cell Biology, Swammerdam Institute for Life Sciences, University of Amsterdam, 1098 XH Amsterdam, The Netherlands

[2]Molecular Biotechnology, Institute of Biology, Leiden University, 2333 BE, Leiden, The Netherlands

[3]Department of Physics and Astronomy and Laser Lab, Free University of Amsterdam, 1081 HV Amsterdam, The Netherlands

[4]Molecular Biophysics, Zernike Institute, University of Groningen, 9747 AG Groningen, The Netherlands

[*]These authors contributed equally to this work.

[#]Corresponding author: Leendert Hamoen, l.w.hamoen@uva.nl

[§]Current address: Division of Chemical Biology, Department of Biology and Biological Engineering, Chalmers University of Technology, 41296 Gothenburg, Sweden

[¤]Current address: Department of Microbiology and Immunobiology, Harvard Medical School, Boston MA 02115, USA

Abstract

Cell division in bacteria is initiated by polymerization of the tubulin homologue FtsZ at midcell. In Gram-positive bacteria FtsZ polymers are anchored to the cell membrane by the protein SepF. Purified *Bacillus subtilis* SepF polymerizes into large rings with an inner diameter of ~40 nm. The biological function of this ring formation is unclear. In this study we have isolated SepF homologues from five different bacterial species and showed that the ability to form rings is conserved. In addition, we found a correlation between the diameter of SepF rings and the thickness of cell division septa. By constructing SepF chimeras, we were able to show that the conserved core domain determines both SepF ring diameter and septum thickness. Our results support a model in which SepF polymers form arc-shaped molecular clamps on the leading edge of nascent septa, thereby controlling septal thickness. This suggests that the intrinsic form of a protein polymer can function as a mold to shape the cell wall.

38 **Introduction**

39

40 Bacterial cell division is accomplished by a complex multi-protein machinery called
41 the divisome. Assembly of the divisome begins with polymerization of the tubulin
42 homologue FtsZ at midcell along the cell membrane, into a ring-like configuration,
43 the so called Z-ring (1). This structure forms a scaffold for the late cell division
44 proteins responsible for synthesis of the dividing septal wall (2). Several cell
45 division proteins support the formation of the Z-ring, and a key step is the
46 anchoring of FtsZ polymers to the cell membrane. This is achieved by the
47 conserved peripheral membrane proteins FtsA and/or SepF. FtsA can be found in
48 both Gram-positive and Gram-negative bacteria, whereas SepF is widely
49 conserved in Gram-positive and cyanobacteria, but has no known homologue in
50 Gram-negatives (3, 4). Several bacteria, such as *Bacillus subtilis*, contain both
51 membrane anchors (5). Both FtsA and SepF directly interact with FtsZ and use an
52 amphipathic α-helix to bind the cell membrane (6, 7).

53 *B. subtilis* can use either FtsA or SepF as anchor for the Z-ring, since only
54 one of them is required for Z-ring formation. However, the absence of SepF results
55 in highly deformed septa, which is not the case when FtsA is absent (4). This
56 indicates that SepF must have an additional function related to septum formation.
57 Curiously, purified *B. subtilis* SepF forms large ring structures with an inner
58 diameter of ~40 nm (Figure 1) (8). Based on the crystal structure of SepF, these
59 rings must encompass at least 80 to 100 SepF molecules (5). *In vitro*, these protein
60 rings are able to bundle FtsZ polymers into very long microtubule-like structures
61 with SepF rings stacked perpendicularly to the FtsZ polymers (9). However, such
62 microtubular structures have never been observed in bacteria. Later studies
63 showed that the membrane-binding amphipathic α-helix of SepF is likely located

64 inside the rings, and it was postulated that SepF might not form rings, but rather
65 forms arcs that wrap over the leading edge of nascent septa, on top of which the
66 FtsZ polymers bind and align (Figure 1) (5). Whether such arcs are formed is
67 unclear since high-resolution electron microscopy is unable to observe this due to
68 the electron density of the bacterial cytoplasm and cell wall.

69 An important argument for the arc model was the realization that the inner
70 diameter of SepF rings (41 nm) is comparable to the thickness of the septal wall
71 (43 nm) (8). Since SepF arcs will control the freedom of movement of FtsZ
72 polymers, including the peptidoglycan synthetic apparatus that is linked to the Z-
73 ring (Figure 1), the diameter of SepF rings would determine the thickness of the
74 septal wall. If this model is correct than (i) the ability to form large protein rings
75 must be a conserved feature of SepF proteins, and (ii) the inner diameter of these
76 rings should correspond to the thickness of division septa. To test this, we purified
77 SepF from different Gram-positive bacteria and found that these proteins also form
78 large protein rings. Importantly, we showed that there is a correlation between
79 SepF ring diameter and septum thickness. Using SepF chimeras, we revealed that
80 the conserved core domain of SepF determines ring diameter. Finally, by
81 expressing these chimeras in *B. subtilis*, we were able to show that changing the
82 core domain also changes septum thickness. These results provided support for
83 the SepF working model presented in Figure 1, and present a possible mechanism
84 how Gram-positive bacteria regulate septum thickness. It also suggests that the
85 intrinsic form of a protein polymer can function as a mold that can shape the cell
86 wall.

87 **Results**

88

89 **SepF rings and tubules**

90 SepF rings have previously been observed with transmission electron microscopy
91 (TEM) using negative staining with uranyl acetate (8). Since high concentrations
92 of this salt might influence the behavior of SepF, we decided to examine whether
93 the protein can form rings under more physiological conditions using atomic force
94 microscopy (AFM). It appeared that under these conditions purified *B. subtilis* SepF
95 also formed rings with diameters of about 40 nm (Figure 2A). Rings were 2 to 4
96 nm high (Figure 2B-D), which corresponds to single or double molecule thick rings,
97 since the crystal packing has shown that SepF polymers can be 1.5 or 2.6 nm
98 thick, depending on the orientation of SepF dimers (8).

99 Previously, SepF was purified as a maltose-binding protein (MBP) fusion,
100 followed by proteolytic cleavage and removal of MBP using ion-exchange
101 chromatography (5, 9). We noticed that after cleavage, SepF precipitates, possibly
102 due to the presence of calcium in the digestion buffer. After resuspension in
103 calcium-free buffer, SepF formed stacks and tubules with diameters corresponding
104 to that of SepF rings when observed by TEM (Figure 2E). After ion-exchange
105 chromatography only rings are found (Figure 2F). These findings, together with
106 the AFM data, show that the circular polymerization of SepF is a robust feature
107 that likely also occurs *in vivo*.

108

109 **SepF from other species**

110 To determine whether ring formation is a conserved feature of SepF, we purified
111 the protein from different Gram-positive organisms. *Bacillus cereus* is an important
112 food-spoiling bacterium (10, 11) and the causative agent of rainforest anthrax

113 (12–14) and was chosen as close relative of *B. subtilis*. We further selected
114 *Clostridium perfringens*, *Mycobacterium tuberculosis*, and *Streptococcus*
115 *pneumoniae,* all of which are important human pathogens. *S. pneumoniae* differs
116 from the rest since it forms cocci instead of rods, and *M. tuberculosis* is one of the
117 bacterial species that lack an FtsA homologue. An amino acid sequence alignment
118 of the different SepF homologues is shown in Figure 3A. The central domain of the
119 protein, which contains the FtsZ binding site (8), is particularly conserved. All
120 proteins were successfully purified as MBP fusions. *C. perfringens, M. tuberculosis,*
121 and *S. pneumoniae* SepF precipitated after proteolytic cleavage from MBP and
122 were further purified by centrifugation, whereas *B. cereus* SepF remained largely
123 soluble and was purified by ion-exchange chromatography.
124
125 **Membrane binding**
126 *B. subtilis* SepF possesses an N-terminal amphipathic α-helix (amino acids 1-13),
127 which targets the protein to the cytoplasmic membrane (5, 6). This N-terminal
128 amphipathic helix is reasonably conserved in the different SepF species (Figure 3A,
129 see Supplementary Figure 1 for helical wheel depictions), although the helices
130 differ in their hydrophobicity and hydrophobic moment (Figure 3B). Nevertheless,
131 when the purified proteins were mixed with artificial liposomes, they caused a
132 strong aggregation of liposomes, and deformed them into small vesicles, as
133 observed with high-resolution structured illumination microscopy (SIM). One
134 example, *S. pneumoniae* SepF, is presented in Figure 3C-D (see Supplementary
135 Figure 2 for all variants). Such liposome deformation is a typical characteristic of
136 membrane-interacting amphipathic α-helices (15), and these data shows that the
137 membrane binding activity of SepF is conserved.
138

139 **Ring formation**

140 If polymerization into a curved structure is an important feature of SepF, this
141 characteristic should not be restricted to the *B. subtilis* protein. To test this, the
142 purified SepF homologues were spotted on TEM grids and negatively stained with
143 uranyl acetate. Indeed, as shown in Figure 4A, all SepF variants formed large rings
144 of a remarkably constant size. However, the average ring diameters varied
145 between species, from ~20 up to ~40 nm (Figure 4B).

146

147 **Correlation with septum thickness**

148 If SepF forms arcs on top of the growing edge of septa, it is likely that the septum
149 thickness corresponds to the diameter of SepF ring (Figure 1). To examine whether
150 such correlation exists, we performed TEM of the different bacterial species and
151 measured the cell wall diameter at the edge of nascent cell division septa (Figure
152 4C-E). Because of its high pathogenicity we used data taken from the literature in
153 case of *M. tuberculosis* (16). A clear correlation was observed between the inner
154 ring diameters and the thickness of the corresponding septa (Figure 4F). Only *B.*
155 *cereus* did not follow this trend, and its SepF rings were smaller than the width of
156 its septa (Figure 4B-E).

157

158 **Core domain defines ring diameter**

159 Proteolytic trimming has shown that the conserved C-terminal domain of *B. subtilis*
160 SepF, spanning amino acids 57 to 151, is sufficient for the formation of rings (5).
161 Therefore, we hypothesized that this core domain determines the ring diameter.
162 To test this, we replaced the conserved core domain of *B. subtilis* SepF with those
163 of the SepF proteins from the other species, maintaining the first 67 and last 13
164 amino acids of *B. subtilis* SepF. These chimeras (16) were then expressed in *E.*

165 *coli*, purified, and visualized by TEM using negative staining. All SepF chimeras
166 were able to form rings, and importantly, the ring diameters of these chimeras
167 corresponded very well to the diameters of the original SepF variants (Figure 5A-
168 D).
169

170 **Functional chimeras**

171 If it is true that the diameter of SepF rings determines the thickness of septa, then
172 expressing a SepF variant with a smaller diameter in *B. subtilis* should result in
173 thinner septa. It is unlikely that SepF from other species function in *B. subtilis*,
174 since the N- and C-termini of SepF, which are much less conserved, are crucial for
175 its activity (5, 9). Therefore, the chimeras provided a unique opportunity,
176 assuming that the core domains are sufficiently conserved so that they can bind
177 *B. subtilis* FtsZ. To test whether these chimeras are active in *B. subtilis*, they were
178 expressed in a Δ*sepF* strain. *B. subtilis* is one of the few species that grows
179 normally in absence of SepF, but its septa are strongly deformed in the absence
180 of this protein (4). This phenotype can be easily observed using high-resolution
181 SIM microscopy by fluorescently labelling of the cell membrane (Figure 6A). Except
182 for the *S. pneumoniae* chimera, the *B. cereus, C. perfringens,* and *M. tuberculosis*
183 chimera were able to restore normal septum formation in the Δ*sepF* background
184 (Figure 6A). This was confirmed by TEM (Figure 6B).

185 The inner ring diameter of the *C. perfringens* SepF chimera (24 nm) is
186 considerably smaller than that of the *B. subtilis* protein (42 nm). When this chimera
187 was expressed in the Δ*sepF* strain, the septum thickness decreased substantially
188 from 43 to 28 nm (Figure 6 C-E). A similar decrease of septum thickness was
189 observed when the *M. tuberculosis* chimera (35 nm diameter) was expressed in
190 the Δ*sepF* background. These results support our hypothesis that the SepF ring

191 diameter controls septum thickness. On the other hand, when we introduced the
192 *B. cereus* chimera in the Δ*sepF* mutant, the septum thickness was comparable to
193 that of wild type cells, whereas the diameter of this chimera is approximately 10
194 nm smaller than that of *B. subtilis* SepF (Figure 6C-E). However, *B. cereus* has an
195 average septum thickness that is comparable to *B. subtilis* (43 and 41 nm,
196 respectively). Thus, this finding is still in line with the conclusion that the central
197 core domain of SepF determines septum thickness.

198 **Discussion**

199

200 In this study we showed (i) that the membrane binding and ring forming activities
201 are conserved in SepF homologues, (ii) that the correlation between ring diameter
202 and septum thickness can be found in different Gram-positive bacteria, and (iii)
203 that the septum thickness of *B. subtilis* cells can be reduced by expressing SepF
204 mutants with a smaller diameter. These findings support the molecular clamp
205 model, in which SepF arcs define the physical constraints for septum thickness
206 (Figure 1). Thus, SepF fulfills a dual function in cell division, anchoring of the Z-
207 ring to the cell membrane and controlling septum thickness.

208 *B. cereus* SepF behaved slightly different and showed an average inner ring
209 diameter of 30 nm, which is smaller than its average septum thickness of 43 nm.
210 Possibly, *B. cereus* SepF polymers are more flexible in a cellular environment,
211 enabling a wider diameter, or there might be other factors involved in controlling
212 septum diameter in this organism in addition to the physical confinement of SepF
213 polymers.

214 Previous structural work has indicated that SepF rings are built of tightly
215 packed dimers. These dimers are formed by two parallel oriented monomers (5),
216 as a consequence of which all SepF dimers have the same orientation in a ring.
217 However, FtsZ polymers treadmill in both directions in the Z-ring (17), and it is
218 likely that they bind SepF rings in both polymer orientations. SepF binds to the C-
219 terminal domain of FtsZ (18), which is connected to the protein by a long flexible
220 linker (19). This flexibility might enable FtsZ polymers with opposite orientations
221 to interact with the same SepF ring.

222 The septal wall of Gram-positive bacteria is build-up of multiple layers of
223 peptidoglycan, and somehow cells are able to carefully control this process,

224 resulting septa with a constant thickness. The SepF clamp model provides a
225 possible explanation for this control mechanism. Many SepF arcs must line the
226 leading edge of the nascent septum to maintain an even thickness. This could be
227 facilitated by the propensity of SepF rings to form stacks (Figure 2E). Gram-
228 negative bacteria contain a cell wall that consists of a single-layer of peptidoglycan.
229 The thickness of this layer is regulated by the outer membrane proteins LpoA and
230 LpoB, which reach through the peptidoglycan layer to contact and regulate the cell
231 membrane-anchored peptidoglycan-synthetic enzymes (20). Possibly, this is why
232 Gram-negative bacteria do not need a SepF-like protein for septum thickness
233 control. It should be mentioned that *E. coli* FtsA has been shown to form ring
234 structures *in vitro* as well (21). However, the inner diameter of these rings is ~15
235 nm, which is considerably smaller than the septum width of *E. coli* (~30-60 nm).
236 Regulation of the shape of septal walls by SepF through its intrinsic
237 curvature is partly reminiscent of the activity of MreB, which controls the rod shape
238 of many bacteria (22). MreB forms polymers of defined curvature that orientate
239 and move transversely to the long axis of cells, along the direction of greatest
240 membrane curvature (23, 24), thereby guiding the cell wall synthetic machinery
241 in a way that enforces and maintains a rod shape (25, 26). However, unlike SepF,
242 the intrinsic curvature of MreB filaments, which has been estimated to have a
243 diameter of roughly 200 nm (23), does not define the diameter of the cell, which
244 is much larger (23). Thus, the control of septum thickness by a molecular clamp
245 appears to be a novel concept of how protein polymers can control the shape of
246 growing cell walls.
247

248 **Material and Methods**

249

250 **Strain construction**

251 All strains used in this study are listed in Supplementary Table 1, plasmids in
252 Supplementary Table 2, and primers in Supplementary Table 3. Plasmids for
253 purification of SepF variants were constructed by PCR amplification of *sepF* from
254 the respective organisms, followed by restriction cloning into the pMalC2 plasmid
255 (27), using the *Xba*I and *Sma*I or *Eco*RI restriction sites. pMalC2-based plasmids
256 for purification of chimera proteins and pAPNC-213-kan-based plasmids (28) for
257 integration of *sepF* variants into the *aprE* locus in the *B. subtilis* genome were
258 constructed by Gibson assembly (29). pMalC2-derived purification plasmids were
259 transformed into calcium-competent *E. coli* BL21 (DE3). pAPNC-213-kan-derived
260 integration plasmids were transformed into *B. subtilis* 168 using a standard
261 starvation protocol (30). Deletions of the *sepF* and *ftsA* genes were introduced by
262 transforming the resulting *B. subtilis* strains with chromosomal DNA isolated from
263 YK204 (*sepF::spc*) (31), BFA2863 (*sepF::ery*) (4), and TB94 (*ftsA::cat*),
264 respectively. TB94 was created by transformation of *B. subtilis* 168 with
265 chromosomal DNA of strain MD133 *ftsA::cat aprE::kan Pspac-ftsA* (31) followed
266 by selection on chloramphenicol resistance but kanamycin sensitivity.

267

268 **Protein purification**

269 *E. coli* BL21 (DE3) strains carrying pMalC2 plasmids for purification of SepF
270 variants were grown overnight in LB containing 100 µg/ml ampicillin at 37 °C under
271 continuous shaking. Cultures were diluted 1:100 and allowed to grow until an OD_{600}
272 of 0.4 in the presence of ampicillin. Expression of maltose-binding protein (MBP)-
273 tagged SepF proteins was induced by addition of 0.5 mM IPTG. Cells were

274 harvested by centrifugation after 4 h of induction and subsequently washed in
275 phosphate-buffered saline supplemented with 1 mM phenylmethylsulfonyl fluoride
276 to prevent protein degradation. Dry cell pellets were flash-frozen in liquid nitrogen
277 and stored at -80 °C until further use. Cell pellets were resuspended in buffer AF
278 (50 mM Tris-HCL, pH 7.4, 200 mM KCl, 5 mM EDTA, 0.5 mM DTT) supplemented
279 with one Complete mini protease inhibitor tablet (Roche) and disrupted by French
280 Press. Cell debris was removed by ultracentrifugation at 31,000 x g, and the
281 resulting supernatant was filtered through 0.2 µm filter membranes prior to
282 loading onto a Tricorn 10/20 column (GE Healthcare) packed with 2 ml amylose
283 resin (New England Biolabs) equilibrated with buffer AF. After loading, the column
284 was washed with 5 column volumes buffer AF, followed by buffer BF (50 mM Tris-
285 HCl, pH 7.4) until the baseline was stable. MBP-tagged SepF variants were eluted
286 with buffer BF containing 10 mM maltose. Appropriate fractions were pooled and
287 digested with factor Xa protease (New England Biolabs) in the presence of 2 mM
288 $CaCl_2$ at 4 °C overnight. *B. cereus* SepF was soluble while the others precipitated
289 after cleavage (*B. subtilis, S. pneumoniae, C. perfringens, M. tuberculosis,* all
290 chimera proteins) due to presence of calcium. Insoluble proteins were separated
291 from soluble MBP and factor Xa by centrifugation at 10,000 x g. Pellets containing
292 pure SepF were dissolved in buffer BF without $CaCl_2$, flash-frozen in liquid nitrogen
293 and stored at -80 °C until further use. SepF variants that were soluble after factor
294 Xa cleavage were separated from MBP and Factor Xa protease by ion exchange
295 chromatography. To this end, digested samples were loaded onto a 1 ml HiTrap Q
296 column (GE Healthcare) equilibrated with buffer BF. The column was washed with
297 buffer BF until the baseline was stable, followed by washing with 7.5% buffer CF
298 (50 mM Tris-HCl, pH 7.4, 1 M KCl) resulting in elution of MBP, and washing with
299 17.5% buffer CF resulting in elution of factor Xa. Pure SepF was eluted with 50%

300 buffer CF, flash-frozen in liquid nitrogen, and stored at -80 °C.

301

302 **Atomic force microscopy**

303 Purified *B. subtilis* SepF was diluted 1:10 in buffer BF and added onto a freshly
304 cleaved highly oriented pyrolytic graphite (HOPG) surface (Agar Scientific) and
305 allowed to settle for 20 min at room temperature prior to imaging in buffer solution
306 (32). Images were taken with an atomic force microscope from Nanotec
307 Electronica (Tres Cantos) operated in jumping mode at room temperature.
308 Olympus OMCL-RC800PSA rectangular, silicon-nitride cantilevers with a nominal
309 tip radius of 15 nm and a nominal spring constant of 0.05 N/m were used. Images
310 were processed and analyzed with WSxM software (33).

311

312 **Fluorescence light microscopy of liposomes**

313 Liposomes were prepared from *E. coli* polar lipid extract (Avanti Polar Lipids) as
314 described previously (6). Liposomes were extruded through 0.2 µm filters.
315 Samples were stained with 1 µg/ml Nile red, spotted on 1.2% agarose films,
316 covered with poly-dopamine-coated cover slips (34), and immediately imaged with
317 a Nikon Eclipse Ti equipped with a CFI Plan Apochromat DM 100x oil objective, an
318 Intensilight HG 130 W lamp, a C11440-22CU Hamamatsu ORCA camera, and NIS
319 elements software. Images were analyzed using ImageJ (National Institutes of
320 Health).

321

322 **Structured illumination (SIM) microscopy**

323 Liposomes for SIM were prepared from *E. coli* polar lipid extract (Avanti Polar
324 Lipids) as described previously (6). Liposomes were extruded through 0.8 µm
325 filters to obtain large enough vesicles. 0.25 mg/ml of the respective SepF variants

326 was mixed with 2 mg/ml liposomes in SepF binding buffer. Samples were stained
327 with 0.5 µg/ml mitotracker green, spotted on 1.2% agarose films, covered with
328 poly-dopamine-coated cover slips (34), and immediately imaged with a Nikon
329 Eclipse Ti N-SIM E microscope setup equipped with a CFI SR Apochromat TIRF
330 100x oil objective (NA1.49), a LU-N3-SIM laser unit, an Orca-Flash 4.0 sCMOS
331 camera (Hamamatsu Photonics K.K.), and NIS elements Ar software. SIM
332 microscopy of bacteria was performed by staining cells with 0.5 µg/ml mitotracker
333 green for 1 min, spotted on a thin film of 1.2% agarose (21).
334

335 **Transmission electron microscopy of proteins**

336 Protein samples were spotted on glow-discharged 200 mesh formvar/carbon-
337 coated copper grids (Agar Scientific) and incubated for 1 min at room temperature.
338 Excess liquid was removed with paper tissue and samples were negatively stained
339 by adding 100 µl 2% uranyl acetate drop by drop. Excess staining solution was
340 removed with paper tissue and samples were allowed to air dry. Samples were
341 examined with a JEOL1010 at 60 kV.
342

343 **Growth conditions for microscopy**

344 *B. cereus, S. pneumoniae*, and *C. perfringens* were grown on tryptic soy agar
345 plates containing 5 % sheep blood (BioMerieux). After three days of aerobic (*B.*
346 *cereus* and *S. pneumoniae*) or anaerobic incubation (*C. perfringens*) at 37 °C,
347 colonies were transferred to fresh plates and incubated for another 48 h prior to
348 suspension in phosphate-buffered saline and preparation for electron microscopy.
349 *B. subtilis* strains were grown in Luria-Bertani (LB) broth at 37 °C under steady
350 agitation. The medium was supplemented with 0.1 mM IPTG to induce expression
351 of SepF variants, where appropriate. It is important not to use more IPTG since

352 SepF overproduction causes membrane deformations that obscure septa (35).
353 Overnight cultures were grown with appropriate antibiotic concentrations (100
354 µg/ml spectinomycin, 10 µg/ml chloramphenicol, 5 µg/ml kanamycin, 1 µg/ml
355 erythromycin), where necessary. Cells were grown until exponential phase (OD_{600}
356 = 0.4) prior to microscopy.
357
358 **Transmission electron microscopy of bacteria**
359 Electron microscopy of bacteria was performed according to van Wezel *at al.*
360 (36)(*B. cereus*, *S. pneumoniae*, *C. perfringens)* or Saeloh *et al.* (37) (*B. subtilis*).
361 Samples were examined with a JEOL 1010 at an electron voltage of 60 kV.
362

Acknowledgements

We gratefully acknowledge Zehui Zhang and Daniel Antwi-berko for help with sample preparation, Wiep Klaas Smits for help with growing strains, Marien P. Dekker and Jan R. T. van Weering for support with TEM, and Gaurav Dugar for critically reading the manuscript. Electron microscopy was performed at the VU/VUMC EM facility, supported by the Netherlands Organization for Scientific Research (NWO, middelgroot 91111009). This work was financially supported by the Netherlands Organization for Scientific Research (NWO, STW-Vici 12128 to LWH and NWO-Vidi to WHR). MW was supported by a postdoc stipend from the Amsterdam Infection and Immunity Institute.

Conflict of Interest

The authors declare that this work was conducted in the absence of any commercial or financial relationships that could be construed as a potential conflict of interest.

Author contributions

MW planned and performed experiments and wrote the paper. INCG constructed strains and performed experiments. YG constructed strains. JW and MGM performed experiments. GJLW and WHR provided tools and planned experiments. LWH designed the study and wrote the paper.

384 **References**

385

386 1. Lutkenhaus J, Pichoff S, Du S (2012) Bacterial cytokinesis: From Z ring to
387 divisome. *Cytoskeleton* 69(10):778–790.
388 2. Gamba P, Veening JW, Saunders NJ, Hamoen LW, Daniel RA (2009) Two-step
389 assembly dynamics of the Bacillus subtilis divisome. *J Bacteriol*
390 191(13):4186–4194.
391 3. Errington J, Daniel RA, Scheffers D-J (2003) Cytokinesis in bacteria. *Microbiol*
392 *Mol Biol Rev* 67(1):52–65, table of contents.
393 4. Hamoen LW, Meile J-C, De Jong W, Noirot P, Errington J (2006) SepF, a novel
394 FtsZ-interacting protein required for a late step in cell division. *Mol Microbiol*
395 59(3):989–999.
396 5. Duman R, et al. (2013) Structural and genetic analyses reveal the protein
397 SepF as a new membrane anchor for the Z ring. *Proc Natl Acad Sci U S A*
398 110(48):E4601-10.
399 6. Strahl H, Hamoen LW (2010) Membrane potential is important for bacterial
400 cell division. *Proc Natl Acad Sci U S A* 107(27):12281–12286.
401 7. Pichoff S, Lutkenhaus J (2005) Tethering the Z ring to the membrane through
402 a conserved membrane targeting sequence in FtsA. *Mol Microbiol*
403 55(6):1722–1734.
404 8. Duman R, et al. (2013) Structural and genetic analyses reveal the protein
405 SepF as a new membrane anchor for the Z ring. *Proc Natl Acad Sci U S A*
406 110(48):E4601-10.
407 9. Gündoğdu ME, et al. (2011) Large ring polymers align FtsZ polymers for
408 normal septum formation. *EMBO J* 30(3):617–626.
409 10. Kotiranta A, Lounatmaa K, Haapasalo M (2000) Epidemiology and

410 pathogenesis of Bacillus cereus infections. *Microbes Infect* 2(2):189–198.
411 11. Bottone EJ (2010) Bacillus cereus, a volatile human pathogen. *Clin Microbiol*
412 *Rev* 23(2):382–398.
413 12. Antonation KS, et al. (2016) Bacillus cereus Biovar Anthracis Causing Anthrax
414 in Sub-Saharan Africa—Chromosomal Monophyly and Broad Geographic
415 Distribution. *PLoS Negl Trop Dis* 10(9):e0004923.
416 13. Hoffmaster AR, et al. (2004) Identification of anthrax toxin genes in a Bacillus
417 cereus associated with an illness resembling inhalation anthrax. *Proc Natl*
418 *Acad Sci* 101(22):8449–8454.
419 14. Hoffmann C, et al. (2017) Persistent anthrax as a major driver of wildlife
420 mortality in a tropical rainforest. *Nature* 548:82.
421 15. Prinz WA, Hinshaw JE (2009) Membrane-bending proteins. *Crit Rev Biochem*
422 *Mol Biol* 44(5):278–291.
423 16. Velayati AA, Farnia P (2016) *Altas of Mycobacterium tuberculosis* (Academic
424 Press, Cambridge). 1st Editio.
425 17. Bisson-Filho AW, et al. (2017) Treadmilling by FtsZ filaments drives
426 peptidoglycan synthesis and bacterial cell division. *Science* 355(6326):739–
427 743.
428 18. Krol E, et al. (2012) Bacillus subtilis SepF binds to the C-terminus of FtsZ.
429 *PLoS One* 7(8):e43293.
430 19. Buske PJ, Mittal A, Pappu R V, Levin PA (2015) An intrinsically disordered
431 linker plays a critical role in bacterial cell division. *Semin Cell Dev Biol* 37:3–
432 10.
433 20. Typas A, et al. (2010) Regulation of peptidoglycan synthesis by outer-
434 membrane proteins. *Cell* 143(7):1097–1109.
435 21. Krupka M, et al. (2017) Escherichia coli FtsA forms lipid-bound minirings that

436 antagonize lateral interactions between FtsZ protofilaments. *Nat Commun*
437 8:15957.
438 22. Jones LJ, Carballido-Lopez R, Errington J (2001) Control of cell shape in
439 bacteria: helical, actin-like filaments in Bacillus subtilis. *Cell* 104(6):913–922.
440 23. Hussain S, et al. (2018) MreB filaments align along greatest principal
441 membrane curvature to orient cell wall synthesis. *Elife* 7:e32471.
442 24. Ursell TS, et al. (2014) Rod-like bacterial shape is maintained by feedback
443 between cell curvature and cytoskeletal localization. *Proc Natl Acad Sci U S A*
444 111(11):E1025-34.
445 25. Dominguez-Escobar J, et al. (2011) Processive movement of MreB-associated
446 cell wall biosynthetic complexes in bacteria. *Science* 333(6039):225–228.
447 26. Garner EC, et al. (2011) Coupled, circumferential motions of the cell wall
448 synthesis machinery and MreB filaments in B. subtilis. *Science*
449 333(6039):222–225.
450 27. Riggs P (2001) Expression and Purification of Maltose-Binding Protein
451 Fusions. *Current Protocols in Molecular Biology* (John Wiley & Sons, Inc.).
452 doi:10.1002/0471142727.mb1606s28.
453 28. Yoshimura M, Oshima T, Ogasawara N (2007) Involvement of the YneS/YgiH
454 and PlsX proteins in phospholipid biosynthesis in both Bacillus subtilis and
455 Escherichia coli. *BMC Microbiol* 7(1):69.
456 29. Gibson DG, et al. (2009) Enzymatic assembly of DNA molecules up to several
457 hundred kilobases. *Nat Meth* 6(5):343–345.
458 30. Hauser PM, Karamata D (1994) A rapid and simple method for Bacillus subtilis
459 transformation on solid media. *Microbiology* 140(7):1613–1617.
460 31. Ishikawa S, Kawai Y, Hiramatsu K, Kuwano M, Ogasawara N (2006) A new
461 FtsZ-interacting protein, YlmF, complements the activity of FtsA during

462 progression of cell division in Bacillus subtilis. *Mol Microbiol* 60(6):1364–
463 1380.
464 32. Heinze K, et al. (2016) Protein Nanocontainers from Nonviral Origin: Testing
465 the Mechanics of Artificial and Natural Protein Cages by AFM. *J Phys Chem B*
466 120(26):5945–5952.
467 33. Horcas I, et al. (2007) WSXM: A software for scanning probe microscopy and
468 a tool for nanotechnology. *Rev Sci Instrum* 78(1):13705.
469 34. te Winkel JD, Gray DA, Seistrup KH, Hamoen LW, Strahl H (2016) Analysis of
470 antimicrobial-triggered membrane depolarisation using voltage sensitive
471 dyes. *Front Cell Dev Biol* 4:29.
472 35. Gao Y, Wenzel M, Jonker MJ, Hamoen LW (2017) Free SepF interferes with
473 recruitment of late cell division proteins. *Sci Rep* 7(1):16928.
474 36. van Wezel GP, et al. (2000) ssgA is essential for sporulation of Streptomyces
475 coelicolor A3(2) and affects hyphal development by stimulating septum
476 formation. *J Bacteriol* 182(20):5653–5662.
477 37. Saeloh D, et al. (2018) The novel antibiotic rhodomyrtone traps membrane
478 proteins in vesicles with increased fluidity. *PLoS Pathog* 14(2):e1006876.
479
480

481 **Figure legends**

482

483 **Figure 1:** SepF working model. *B. subtilis* SepF forms large rings with an average
484 inner ring diameter (d) of 41 nm. The septum thickness (t) of *B. subtilis* cells
485 measures on average 43 nm. A crossection of a developing septum (grey) is
486 depicted. FtsZ polymers (Z) bind to the outside of SepF rings, and the
487 transmembrane peptidoglycan synthesis machinery (P) is associated with FtsZ
488 polymers. Of note, it is not yet know how these transmembrane proteins are linked
489 to the FtsZ polymers in Gram-positive bacteria, and this association might be
490 indirect.

491

492 **Figure 2:** SepF rings and tubules. **(A)** Plane AFM images of three different SepF
493 rings imaged in buffer solution. **(B)** 3D projections of the same images. **(C)** Height
494 measurements of the individual SepF rings shown in A and B. **(D)** Height
495 measurements of SepF rings derived from AFM data. **(E)** TEM image of SepF stack
496 and tubules after cleavage from MBP. **(F)** TEM image of SepF rings after ion-
497 exchange chromatography. Scale bars 100 nm.

498

499 **Figure 3:** Membrane binding of SepF is conserved. **(A)** Sequence alignment
500 (Clustal Omega) of SepF homologues used in this study. Dark grey marks identical,
501 light grey similar amino acids. Arrows mark the highly conserved core domain of
502 SepF. **(B)** Hydrophobic moment plot of the putative N-terminal α-helices of SepF
503 homologues. High H values indicate strong hydrophobicity. The hydrophobic
504 moment (μH) is a measure for the amphipathicity of an α-helix (high values
505 indicating strong amphipathicity). The plot of H and μH indicates the probability of
506 an α-helix to reside in the globular or surface-exposed domains of a protein and

507 can be used to predict transmembrane or amphipathic membrane-binding helices.
508 Black dots indicate known globular (*Bacillus thermoproteolyticus* thermolysin, aa
509 67-88), transmembrane (*B. subtilis* EzrA, aa 1-21) and amphipathic (*B. subtilis*
510 FtsA, aa 424-440) helices for comparison. N-terminal α-helices of SepF
511 homologues are depicted in red. **(C)** Fluorescence light microscopy images
512 showing the aggregation of small liposomes (~200 nm) stained with Nile red. **(D)**
513 Structured illumination microscopy images showing deformation of large liposomes
514 (800 nm) stained with mitotracker green. 0.25 µg/ml of the respective SepF
515 proteins were mixed with 2 mg/ml liposomes. See Supplementary Figure 2 for the
516 results with other SepF variants. Scale bars 1 µm.
517
518 **Figure 4:** Correlation between SepF ring diameter and septum thickness. **(A)** TEM
519 pictures of purified SepF from the different species. Scale bar 50 nm. **(B)**
520 Quantification of the inner SepF ring diameter. Black bars show mean with
521 standard error of the mean. A minimum of 45 rings was measured. **(C)** TEM images
522 of nascent cell division septa of the respective species. **(D)** Quantification of the
523 thickness of the nascent septa of the respective organisms. Black bars show mean
524 with standard error of the mean. A minimum of 50 septa was measured. **(E)**
525 Comparison of inner ring diameters with nascent septum thickness. Average +/-
526 standard deviations are indicated. *Data for *M. tuberculosis* were taken from the
527 literature (16). **(F)** Correlation between inner SepF ring diameter and septum
528 thickness.
529
530 **Figure 5:** The conserved core domain of SepF determines ring diameter. **(A)** TEM
531 pictures of purified SepF chimera proteins. **(B)** Quantification of ring diameter.
532 Black bars represent mean with standard error of the mean. A minimum of 50

533 rings was measured. **(C)** Comparison of the inner ring diameters of the original
534 and chimera proteins. Average +/- standard deviation are given. **(D)** Correlation
535 between original and chimera ring diameter.
536
537 **Figure 6:** SepF ring diameter determines septum thickness. **(A)** SIM images of *B.*
538 *subtilis* Δ*sepF* cells expressing different SepF chimera driven by the IPTG-inducible
539 *Pspac* promotor. Cells were grown in the presence of 100 µM IPTG until mid-log
540 phase prior to membrane staining and microscopy. Lack of SepF results in severely
541 deformed septa, which appear as highly fluorescent membrane patches due to
542 membrane invaginations and double membranes. Scale bar 2 µm. **(B)**
543 Representative TEM images of septa of Δ*sepF* strains expressing the different SepF
544 chimeras. Scale bar 1 µm. **(C)** Quantification of the septum thickness of the
545 different strains. Black bars represent mean with standard error of the mean. p
546 values for *C. perfringens* and *M. tuberculosis* chimeras compared to *B. subtilis* are
547 <0.0001. **(D)** Comparison and **(E)** correlation of the inner ring diameter of SepF
548 chimeras and nascent septum thickness of *B. subtilis* Δ*sepF* expressing the
549 chimeras.
550

551 **Figure 1.**

552

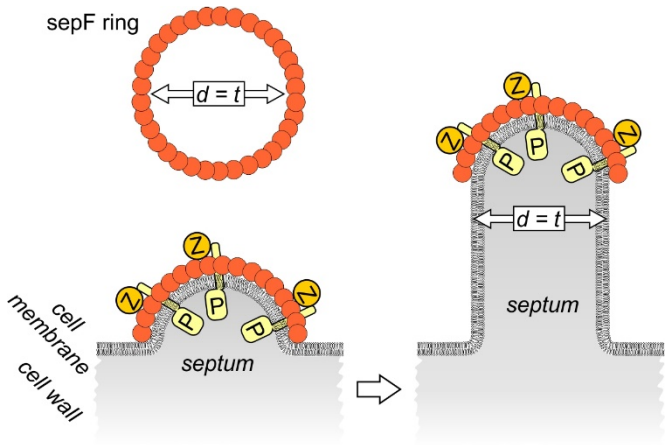

553 **Figure 2.**

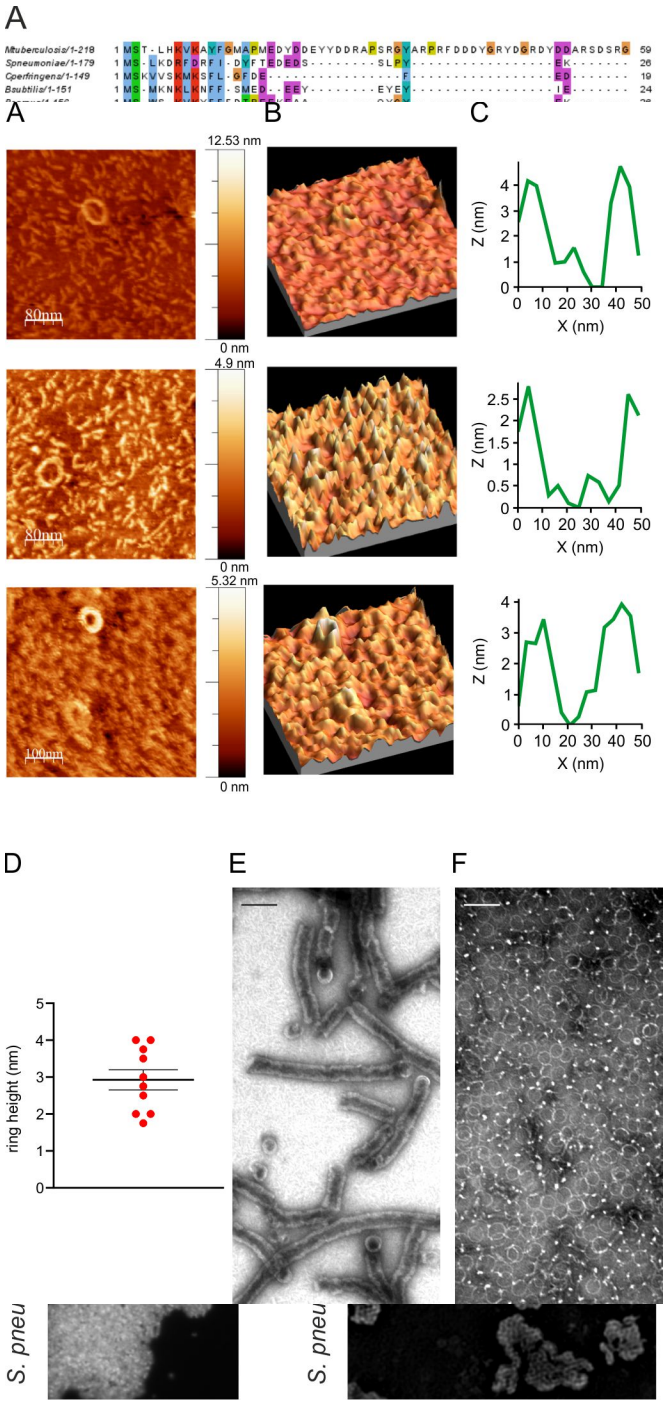
A
Mtuberculosis/1-218
Spneumoniae/1-179
Cperfringens/1-149
Bsubtilis/1-151
A
B
C
12.53 nm
0 nm
80nm
4.9 nm
0 nm
80nm
5.32 nm
0 nm
100nm
Z (nm)
X (nm)
D
E
F
ring height (nm)
S. pneu
S. pneu

554 **Figure 3.**

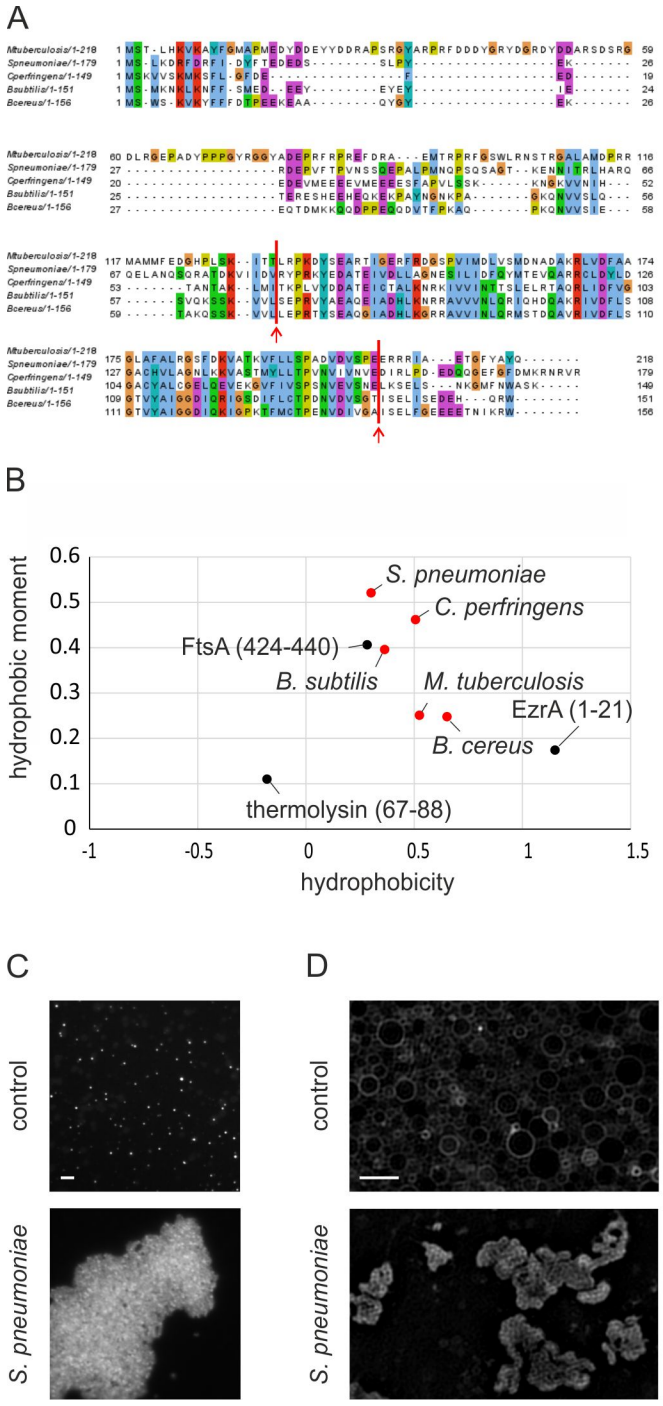
A
Mtuberculosis/1-218
Spneumoniae/1-179
Cperfringens/1-149
Bsubtilis/1-151
Bcereus/1-156
B
hydrophobic moment
hydrophobicity
S. pneumoniae
C. perfringens
FtsA (424-440)
B. subtilis
M. tuberculosis
EzrA (1-21)
B. cereus
thermolysin (67-88)
C
D
control
S. pneumoniae

555 **Figure 4.**

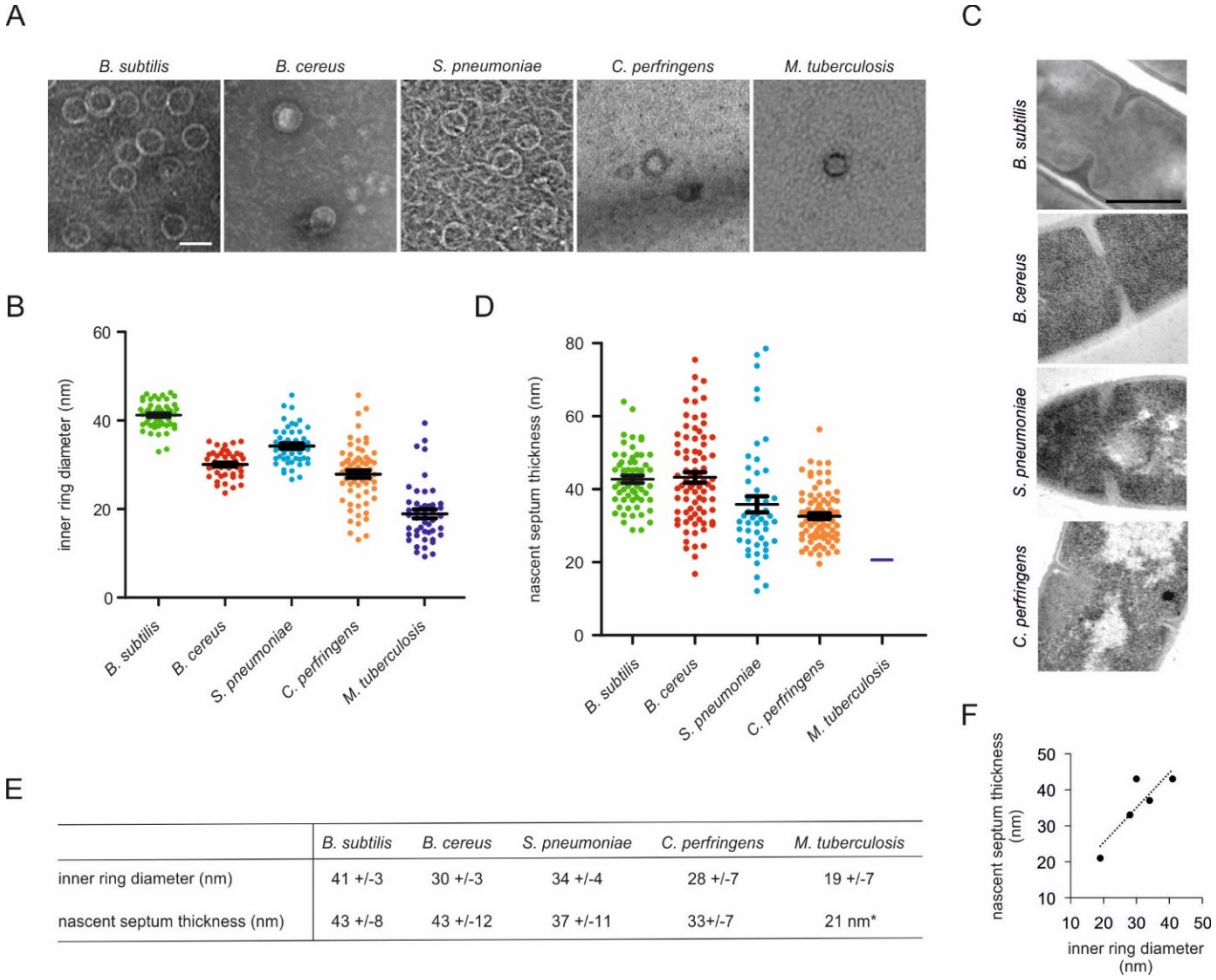

E

	B. subtilis	*B. cereus*	*S. pneumoniae*	*C. perfringens*	*M. tuberculosis*
inner ring diameter (nm)	41 +/-3	30 +/-3	34 +/-4	28 +/-7	19 +/-7
nascent septum thickness (nm)	43 +/-8	43 +/-12	37 +/-11	33+/-7	21 nm*

556 **Figure 5.**

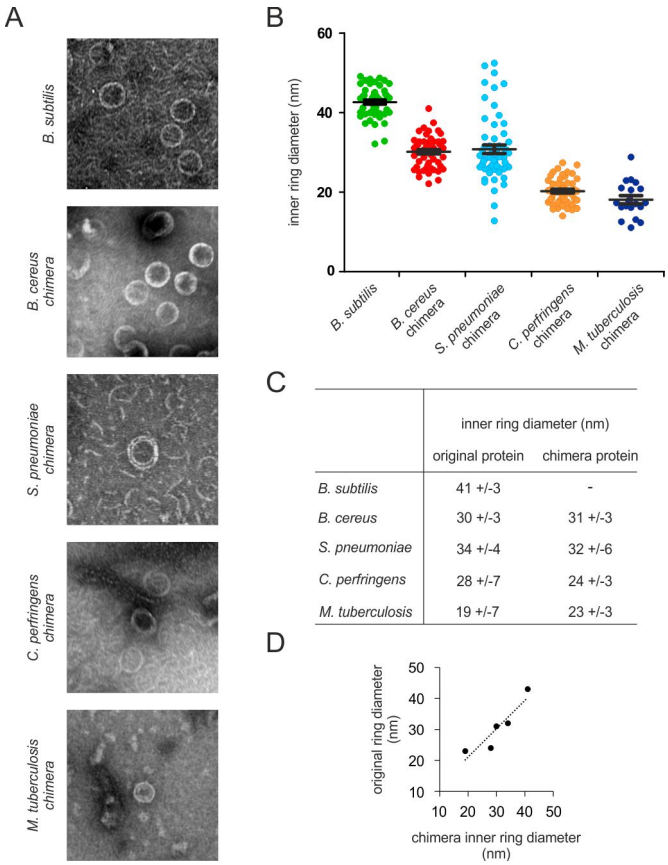

	inner ring diameter (nm)	
	original protein	chimera protein
B. subtilis	41 +/-3	-
B. cereus	30 +/-3	31 +/-3
S. pneumoniae	34 +/-4	32 +/-6
C. perfringens	28 +/-7	24 +/-3
M. tuberculosis	19 +/-7	23 +/-3

557 **Figure 6.**

A

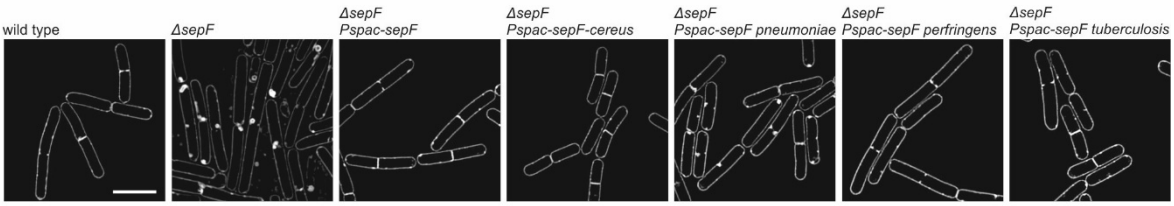

B

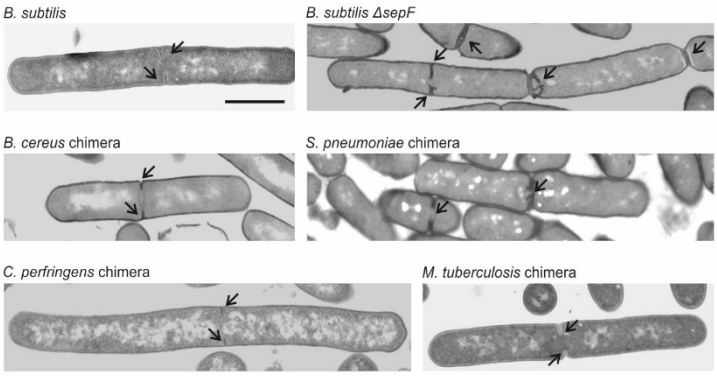

C

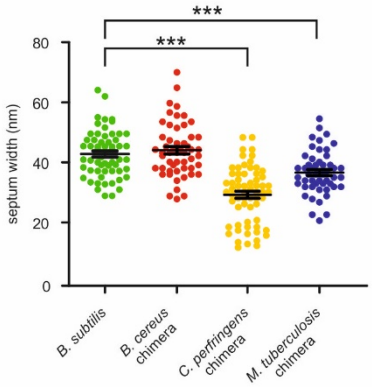

D

	B. subtilis	B. cereus	C. perfringens	M. tuberculosis
inner ring diameter chimeras (nm)	41 +/-3	31 +/-3	24 +/-3	23 +/-3
nascent septum thickness chimeras (nm)	43 +/-8	44 +/-9	28 +/-7	35 +/-10
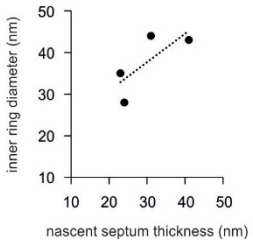
E